SOC Estimation of Lithium-Ion Battery Pack Considering Balancing Current

Zhiliang Zhang, *Senior Member, IEEE*, Xiang Cheng, Zhou-Yu Lu, and Dong-Jie Gu

***Abstract*—The state-of-charge (SOC) estimation approaches based on the pack model can hardly provide precise estimation due to cell difference, while the approaches based on each cell cost high computation resource, which are not suitable for real-time application. The estimation error can be further enlarged without considering balancing current. The SOC estimation approach of the battery pack considering balancing current is proposed, which dynamically searches for the cell with maximum or minimum voltage, and it only needs to calculate the selected cell in every estimation cycle. Compared to the approaches based on the pack model or each single cell, this approach can achieve precise pack SOC and cost less calculation time and resource. It has been verified with ten series-connected 200 Ah Li(NiCoMn)O_2 batteries. The SOC estimation error is limited to 0.3% during the charging process, and a reduction of 2.5% is achieved compared to an error of 2.8% based on the pack model. A reduction of 1% is achieved compared to an error of 1.5% based on the pack model during the discharging process. Compared to an error of 1.7% without considering balancing current, a reduction of 1.4% is achieved during the charging process.**

***Index Terms*—Adaptive extended Kalman filter, battery pack, balancing current, state of charge (SOC).**

I. Introduction

MANY methods have been proposed to estimate the state of charge (SOC) of battery pack. The typical approaches based on the pack model ignore the difference among cells so that SOC of some cell could be higher or lower than pack SOC. The approaches based on each cell can estimate cell SOC accurately. Unfortunately, for the pack with a massive amount of cells, these methods cost high calculation resource so that they are hardly applied to real-time application. At the same time, the balancing current in the equalization circuit affects cell SOC, and it needs be discussed and considered carefully.

In this paper, the dynamic voltage-based SOC estimation approach of battery pack considering balancing current is proposed. This approach dynamically searches for $V_{\max}$ or $V_{\min}$ cell, and the pack SOC is estimated based on $V_{\max}$ cell in charging process and $V_{\min}$ cell in discharging process. It is based on adaptive extended Kalman filter (AEKF) so that the SOC estimation precision can be guaranteed. This method is also convenient to be programmed in the microcontroller unit (MCU) and implemented in the battery management system (BMS). Different from the approaches based on each cell, this approach can reduce the computation time, and it is suitable for the real-time application. This approach has been validated with the experiment on ten series-connected Li(NiCoMn)O_2 batteries. Each cell has the rated capacity of 200 Ah and rated voltage of 3.6 V. The SOC estimation error is limited within 0.3% during the charging process. Compared to an error of 2.8% based on the pack model, an error reduction of 2.5% is achieved. An error reduction of 1% is achieved compared to an error of 1.5% based on the pack model during the discharging process. Compared to an error of 1.7% without considering balancing current, an error reduction of 1.4% is achieved during the charging process.

Manuscript received September 22, 2016; revised January 10, 2017 and March 14, 2017; accepted April 20, 2017. Date of publication May 2, 2017; date of current version December 1, 2017. This work was supported by the Natural Science Foundation of China under Grant 51577089 and the Top Talents Foundation of Jiangsu Province. Recommended for publication by Associate Editor O. Trescases. *(Corresponding Author: Zhiliang Zhang.)*

Z. Zhang, X. Cheng, and Z.-Y. Lu are with the Aero-Power Sci-Tech Center, Nanjing University of Aeronautics and Astronautics, Nanjing 210007, China (e-mail: zlzhang@nuaa.edu.cn; chengxiang@nuaa.edu.cn; luzy@nuaa.edu.cn).

D.-J. Gu was with the Aero-Power Sci-Tech Center, Nanjing University of Aeronautics and Astronautics, Nanjing 210007, China. He is now with the Department of Power Electronics Center, Delta Electronics, Shanghai 200120, China (e-mail: dongjiegu@nuaa.edu.cn).

Color versions of one or more of the figures in this paper are available online at http://ieeexplore.ieee.org.

Digital Object Identifier 10.1109/TPEL.2017.2700324

II. Analysis of the Basic Battery Pack SOC Estimation Approaches

A. SOC Estimation Approaches Based on the Battery Pack Model

The approaches based on the pack model ignore the difference among cells [1]. Some cell SOC could be higher or lower than the pack SOC. The screening process has been proposed to select cells that have similar electrochemical characteristics [2]. The pack SOC can be estimated by EKF based on the simplified pack model. The approach based on discrete wavelet transform (DWT) is proposed in [3]. The DWT is utilized to analyze and evaluate the measured charging and discharging voltage. Then, dual EKF (DEKF) is applied to estimate pack SOC.

These approaches can provide precise SOC of battery pack composed by similar cells. They can also reduce the calculation time because they are based on the simplified pack model rather than each cell. Unfortunately, the difference of electrochemical characteristics normally happens with repeated charging and discharging process, and these approaches are not applicable to the cells with low consistency.

B. SOC Estimation Approaches Based on Each Battery Cell

The method that utilizes the equalization circuits to estimate cell's voltage and current is proposed in [4]. It can estimate cell SOC by the block data iterative search algorithm and recursive

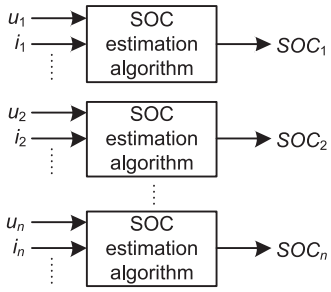

Fig. 1. SOC estimation based on each battery cell.

estimation algorithm. The accuracy is influenced by high ratio of bypass resistance to cell internal resistance. An improved method based on the pack voltage and the cell internal resistance is proposed in [5]. The newton observer is designed to obtain cell SOC. In [6], a reliable pack SOC estimation approach is proposed, by which the cell impedance and SOC variation can be detected accurately. Unfortunately, the detailed process of how to determine the tunable correction gain was not discussed.

The process of SOC estimation based on battery cell is shown in Fig. 1. u_n and i_n is the voltage and current of Cell #*n*. SOC_n is SOC of Cell #*n*. It can be observed that these approaches estimate SOC based on the voltage, current and other information. However, they require massive computation resource especially for the battery pack with large amounts of cells.

C. SOC Estimation Approaches of Battery Pack With Equalization Circuits

The equalization strategy used in the battery pack can be summarized into two categories: 1) voltage-based strategy; 2) SOC-based strategy. In [7] and [8], the battery pack is balanced according to the terminal voltage of each cell. The cell SOC is estimated based on open circuit voltage (OCV)–SOC curve. However, the flat area of the OCV–SOC curve normally exists in the lithium-ion batteries. It can be known that the cells with small OCV difference could have large SOC difference. This characteristic has strong effect on balancing performance and voltage-based SOC estimation. In [9], [10], the cells are balanced according to cell SOC. However, the cell SOC is calculated based on the OCV–SOC curve. As a result, these approaches are similar to the voltage-based approaches and they suffer from the similar disadvantages. The current integration technique is used in [11]–[13]. Unfortunately, these approaches cannot compensate for SOC estimation error caused by the inaccuracy of the sampled current.

III. Proposed Dynamic Voltage-Based SOC Estimation Approach

A. Definition of Pack SOC

The battery pack SOC is defined as

$$\mathrm{SOC}_{\mathrm{pack}} = \begin{cases} \mathrm{SOC}_{V_{\max}}, & \text{charging process} \\ \mathrm{SOC}_{V_{\min}}, & \text{discharging process} \end{cases} \quad (1)$$

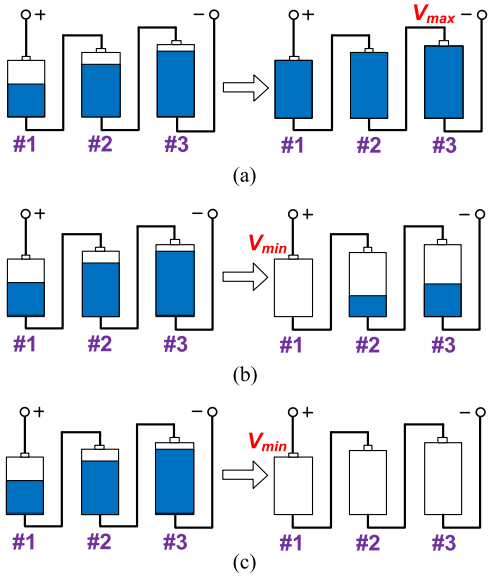

Fig. 2. Charge and discharge with passive or active equalization: (a) charge (passive/active equalization), (b) discharge (passive equalization), and (c) discharge (active equalization).

where $\mathrm{SOC}_{\mathrm{pack}}$ is the pack SOC, $\mathrm{SOC}_{V_{\max}}$ is the SOC of $V_{\max}$ cell, and $\mathrm{SOC}_{V_{\min}}$ is the SOC of $V_{\min}$ cell.

Fig. 2(a) shows the charging process with passive or active equalization. Fig. 2(b) shows the discharging process with passive equalization. Fig. 2(c) presents the discharging process with active equalization.

It is assumed that Cell #3 reaches to the maximum limit voltage in Fig. 2(a). It can be known that the cells in the pack can be fully charged. To avoid over-charge, the pack cannot be charged anymore and pack SOC can be considered as 100%. The voltage of Cell #3 is $V_{\max}$ and its SOC is 100%. Therefore, the $V_{\max}$ cell decides the end of charging process, and the pack SOC can be defined as SOC of $V_{\max}$ cell.

It is assumed that Cell #1 reaches to the minimum limit voltage in Fig. 2(b) and (c). It should be noted that some cells in Fig. 2(b) cannot be fully discharged. It is because that the passive equalization is not applied during the discharging process. Different from Fig. 2(b), all cells in Fig. 2(c) can be fully discharged owing to the application of active equalization. To avoid over-discharge, the pack cannot be discharged anymore and pack SOC can be considered as zero. It is noted that the voltage of Cell #1 is $V_{\min}$ and its SOC is zero. Therefore, the $V_{\min}$ cell decides the end of discharging process, and the pack SOC can be defined as SOC of $V_{\min}$ cell.

B. Proposed SOC Estimation Approach

The $V_{\max}$ and $V_{\min}$ cell with equalization circuit is shown in Fig. 3. It can be noted that the $V_{\max}$ cell could be discharged to balance its SOC during the charging process, and the $V_{\min}$ cell could be charged or not (dependent on active or passive equalization) to balance its SOC. Therefore, the balancing current should be considered carefully in cell SOC estimation.

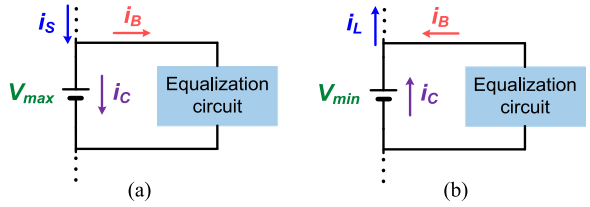

Fig. 3. (a) $V_{\max}$ cell in charging process. (b) $V_{\min}$ cell in discharging process.

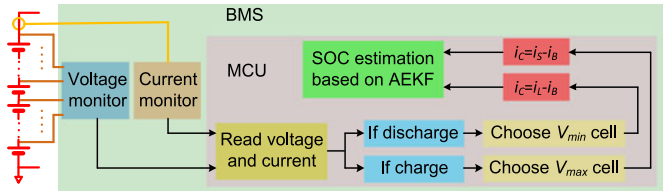

Fig. 4. Block diagram of proposed approach.

From Fig. 3(a), for the charging process, the cell current i_C of the $V_{\max}$ cell can be obtained as

$$i_C = i_S - i_B \tag{2}$$

where i_C is the actual current in battery cell, i_S is the charging current, and i_B is the balancing current.

From Fig. 3(b), for the discharging process, the cell current i_C of the $V_{\min}$ cell can be obtained as

$$i_C = i_L - i_B \tag{3}$$

where i_L is the discharging current. i_B is zero when the passive equalization is applied.

The procedure of the proposed approach is shown in Fig. 4. This approach dynamically searches for $V_{\max}$ cell in charging process or $V_{\min}$ cell in discharging process. After obtaining the voltage and current of $V_{\max}$ or $V_{\min}$ cell, they are applied to AEKF and the pack SOC can be estimated accurately.

IV. Analysis of Proposed Approach and Principle of Operation

A. Analysis of Proposed Approach With Passive Equalization

For the passive equalization, a threshold of voltage difference is set to select cells which need to be balanced, and the terminal voltage of each cell is compared to $V_{\min}$. If the voltage difference is higher than the threshold, this cell needs to be discharged. It can be mathematically described as

$$\begin{cases} V_{\text{cell}} - V_{\min} > V_{\text{th}}, & \text{discharging balance} \\ \text{Others}, & \text{no balance} \end{cases} \tag{4}$$

where V_{cell} is the terminal voltage and V_{th} is the threshold of voltage difference and it is positive.

The passive equalization during the charging and discharging process is shown in Fig. 5(a) and (b). i_{Bn} is the balancing current of Cell #n. In practical application, the passive equalization is normally utilized in the charging process.

It is assumed that Cell #1 is the $V_{\max}$ cell and Cell #$(n-1)$ is the $V_{\min}$ cell. From Fig. 5(a), it can be observed that the current via $V_{\max}$ cell contains the balancing current

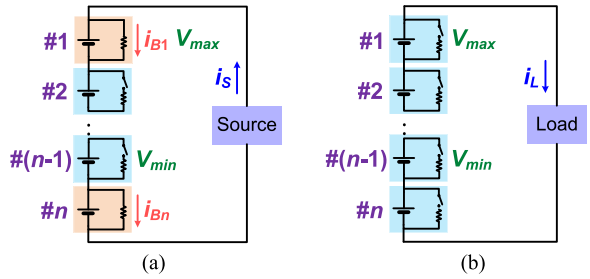

Fig. 5. (a) Passive equalization during charging process. (b) Passive equalization during discharging process.

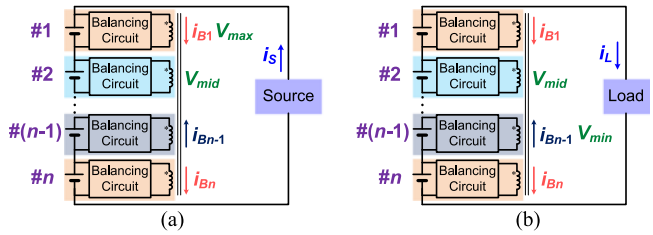

Fig. 6. (a) Active equalization during charging process. (b) Active equalization during discharging process.

i_{B1}. To estimate SOC of $V_{\max}$ cell, the balancing current i_{B1} should be considered carefully. From Fig. 5(b), it can be observed that the current via $V_{\min}$ cell is only the load current i_L, Therefore, SOC estimation of $V_{\min}$ cell can ignore the balancing current.

B. Analysis of Proposed Approach With Active Equalization

The active equalization realizes cell balance by transferring the redundant charge from the cell with higher voltage to the cell with lower voltage, and the Middle Voltage (V_{mid}) cell can be used as the reference. The terminal voltage of each cell is compared to V_{mid}. If the voltage difference is higher than V_{th}, this cell needs to be discharged or charged. On the other hand, the cell whose voltage difference is lower than V_{th} needs no operation. It can be described as

$$\begin{cases} V_{\text{cell}} - V_{\text{mid}} > V_{\text{th}} & \text{discharging balance} \\ V_{\text{cell}} - V_{\text{mid}} < -V_{\text{th}} & \text{charging balance} \\ \text{others} & \text{no balance} \end{cases} \tag{5}$$

To analyze the balancing current, the active equalization during the charging and discharging process is shown in Fig. 6(a) and Fig. 6(b). It is assumed that Cell #$(n-1)$, #1 and #2 is $V_{\min}$, $V_{\max}$ and V_{mid} battery cell.

From Fig. 6(a), it can be observed that the current that flows through $V_{\max}$ cell contains the discharging balancing current i_{B1}. From Fig. 6(b), it can be observed that the current that flows through $V_{\min}$ cell contains the charging balancing current i_{Bn-1}. To estimate SOC of $V_{\max}$ and $V_{\min}$ battery cell, the balancing current needs to be taken into consideration.

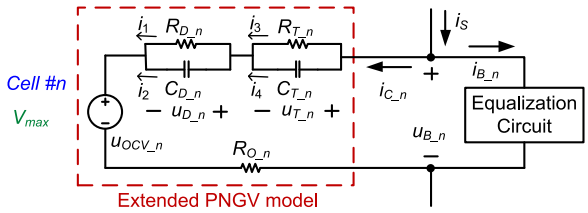

Fig. 7. PNGV model with equalization circuit during charging process.

V. Model Derivation and Flowchart of Proposed Approach

A. Derivation of AEKF Considering Balancing Current

To estimate the SOC of $V_{\max}$ and $V_{\min}$ cell, AEKF and the extended partnership for new generation of vehicles (PNGV) model is used in this approach. The structure of this model with equalization circuit is shown in Fig. 7. It shows Cell #*n* in the pack during the charging process, and it is assumed that Cell #*n* is $V_{\max}$ cell. u_{OCV_n} is OCV of Cell #*n*. R_{O_n} is the internal resistance. R_{D_n}, R_{T_n}, C_{D_n} and C_{T_n} are the polarization resistances and polarization capacitances. i_S is the charging current. i_{B_n} is the balancing current. i_{C_n} is the actual current that flows through Cell #*n*. i_1, i_2, i_3, and i_4 are the branch current. u_{D_n} and u_{T_n} are the voltage of polarization resistance R_{D_n} and R_{T_n}. u_{B_n} is the terminal voltage of Cell #*n*.

From Fig. 7, according to KCL and KVL, (6) and (7) can be derived as

$$i_{C\_n} - i_1 = R_{D\_n} C_{D\_n} \frac{di_1}{dt} \tag{6}$$

$$i_{C\_n} - i_3 = R_{T\_n} C_{T\_n} \frac{di_3}{dt}. \tag{7}$$

Suppose "*s*" as the Laplace operator, the Laplace transform of (6) and (7) can be derived as

$$\frac{I_1(s)}{I_{C\_n}(s)} = \frac{1}{1 + R_{D\_n} C_{D\_n} s} \tag{8}$$

$$\frac{I_3(s)}{I_{C\_n}(s)} = \frac{1}{1 + R_{T\_n} C_{T\_n} s} \tag{9}$$

where $I_1(s)$, $I_3(s)$, and $I_{C\_n}(s)$ are the Laplace transforms of i_1, i_3, and i_{C_n}, respectively.

It is assumed that in the period $t_{k-1} - t_k$, $di_{C\_n}/dt = 0$. The Laplace transforms of u_{D_n} and u_{T_n} are derived as

$$U_{D\_n}(s) = \frac{1}{1 + \tau_{D\_n} s} \cdot \frac{i_{C\_n}}{s} \cdot R_{D\_n} \tag{10}$$

$$U_{T\_n}(s) = \frac{1}{1 + \tau_{T\_n} s} \cdot \frac{i_{C\_n}}{s} \cdot R_{T\_n} \tag{11}$$

where $U_{D\_n}(s)$ and $U_{T\_n}(s)$ are the Laplace transforms of u_{D_n} and u_{T_n}, respectively. τ_{D_n} and τ_{T_n} are the time constants of $R_{D\_n} C_{D\_n}$ and $R_{T\_n} C_{T\_n}$ circuits, respectively.

According to the aforementioned expressions, the zero-state voltage responses of $R_{D\_n} C_{D\_n}$ and $R_{T\_n} C_{T\_n}$ circuits under i_{C_n} at time *k* are derived as

$$u^k_{D\_n,\mathrm{zerostate}} = i^{k-1}_{C\_n} R_{D\_n} \cdot [1 - \exp(-\Delta t/\tau_{D\_n})] \tag{12}$$

$$u^k_{T\_n,\mathrm{zerostate}} = i^{k-1}_{C\_n} R_{T\_n} \cdot [1 - \exp(-\Delta t/\tau_{T\_n})] \tag{13}$$

where Δt is the sampling period of the voltage and current.

The zero-input voltage responses of $R_{D\_n} C_{D\_n}$ and $R_{T\_n} C_{T\_n}$ circuits at time *k* are derived as

$$u^k_{D\_n,\mathrm{zeroinput}} = u^{k-1}_{D\_n} \cdot \exp\left(-\Delta t/\tau_{D\_n}\right) \tag{14}$$

$$u^k_{T\_n,\mathrm{zeroinput}} = u^{k-1}_{T\_n} \cdot \exp\left(-\Delta t/\tau_{T\_n}\right). \tag{15}$$

Therefore, the total voltage responses of $R_{D\_n} C_{D\_n}$ and $R_{T\_n} C_{T\_n}$ circuits at time *k* are obtained as

$$u^k_{D\_n} = i^{k-1}_{C\_n} R_{D\_n} \cdot [1 - \exp(-\Delta t/\tau_{D\_n})] + u^{k-1}_{D\_n} \cdot \exp\left(-\Delta t/\tau_{D\_n}\right) \tag{16}$$

$$u^k_{T\_n} = i^{k-1}_{C\_n} R_{T\_n} \cdot [1 - \exp(-\Delta t/\tau_{T\_n})] + u^{k-1}_{T\_n} \cdot \exp\left(-\Delta t/\tau_{T\_n}\right). \tag{17}$$

For the charging process, SOC of Cell #*n* at time *k* can be estimated by

$$SOC^k = SOC^{k-1} + \frac{\eta \Delta t}{C_{\mathrm{nom}}} \times i^{k-1}_{C\_n} \tag{18}$$

where C_{nom} is the nominal capacity of Cell #*n* and η is the coulombic efficiency.

According to KVL, the terminal voltage of Cell #*n* at time *k* is obtained as

$$u^k_{B\_n} = u^k_{\mathrm{OCV}\_n} + i^k_{C\_n} R_{O\_n} + u^k_{D\_n} + u^k_{T\_n}. \tag{19}$$

The battery is a typical nonlinear system, and it can be modeled as

$$x_{k+1} = f(x_k, u_k) + w_k \tag{20}$$

$$y_k = h(x_k, u_k) + v_k \tag{21}$$

where $f(x_k, u_k)$ is the state transition function and $h(x_k, u_k)$ is the measurement function. w_k and v_k are the zero-mean white Gaussian stochastic processes. x_k is the state vector, and u_k and y_k are the input and the output, respectively.

Taking SOC, u_{D_n} and u_{T_n} as the state variables, the state vector at time *k* is

$$x_k = \begin{bmatrix} \mathrm{SOC}^k & u^k_{D\_n} & u^k_{T\_n} \end{bmatrix}^T. \tag{22}$$

According to KCL, the current via Cell #*n* at time *k* can be obtained as

$$i^k_{C\_n} = i^k_S - i^k_{B\_n}. \tag{23}$$

Based on the aforementioned analysis, the state transition function and the measurement function are obtained as

$$x_{k+1}=\begin{bmatrix}1 & 0 & 0\\ 0 & \exp\left(-\Delta t/\tau_{D\_n}\right) & 0\\ 0 & 0 & \exp\left(-\Delta t/\tau_{T\_n}\right)\end{bmatrix}\times\begin{bmatrix}SOC^k\\ u^k_{D\_n}\\ u^k_{T\_n}\end{bmatrix}+\begin{bmatrix}+\dfrac{\eta\Delta t}{C_{\rm nom}}\\ R_{D\_n}[1-\exp\left(-\Delta t/\tau_{D\_n}\right)]\\ R_{T\_n}[1-\exp\left(-\Delta t/\tau_{T\_n}\right)]\end{bmatrix}\times\left(i^k_S-i^k_{B\_n}\right) \tag{24}$$

$$y_k=\begin{bmatrix}1 & 1 & 1\end{bmatrix}\times\begin{bmatrix}u^k_{{\rm OCV}\_n}\\ u^k_{D\_n}\\ u^k_{T\_n}\end{bmatrix}+\left(i^k_S-i^k_{B\_n}\right)\times R_{O\_n}. \tag{25}$$

At each time step, $f(x_k, u_k)$ and $h(x_k, u_k)$ are linearized by the first-order Taylor-series expansion given that they are differentiable at all operating points and

$$A_k=\left.\frac{\partial f}{\partial x}\right|_{x=\hat{x}^+_k} \tag{26}$$

$$C_k=\left.\frac{\partial h}{\partial x}\right|_{x=\hat{x}^-_k} \tag{27}$$

where A_k is the transition matrix and C_k is the observation matrix. A superscript "−" denotes a priori estimation while a superscript "+" denotes a posteriori estimation. A superscript "^" denotes a state estimation.

According to the aforementioned equation, A_k and C_k can be derived as

$$A_k=\begin{bmatrix}1 & 0 & 0\\ 0 & \exp\left(-\Delta t/\tau_{D\_n}\right) & 0\\ 0 & 0 & \exp\left(-\Delta t/\tau_{T\_n}\right)\end{bmatrix} \tag{28}$$

$$C_k=\left[\left.\frac{du_{{\rm OCV}\_n}}{d{\rm SOC}}\right|_{{\rm SOC}=\widehat{\rm SOC}^-_k}\quad 1\quad 1\right]. \tag{29}$$

The procedure of AEKF is introduced as follows. During the prediction procedure, AEKF predicts the state value and updates the state uncertainty

$$\hat{x}^-_k=f(\hat{x}^+_{k-1},u_{k-1}) \tag{30}$$

$$\Sigma^-_{x_k}=A_{k-1}\Sigma^+_{x_{k-1}}A^T_{k-1}+Q_{k-1} \tag{31}$$

where Σ_x is the state covariance matrix and Q_k is the process noise covariance matrix.

Then, the Kalman gain vector L_k can be obtained as

$$L_k=\Sigma^-_{x_k}C^T_k\left(C_k\Sigma^-_{x_k}C^T_k+R_k\right)^{-1} \tag{32}$$

where R_k is the measurement noise covariance matrix.

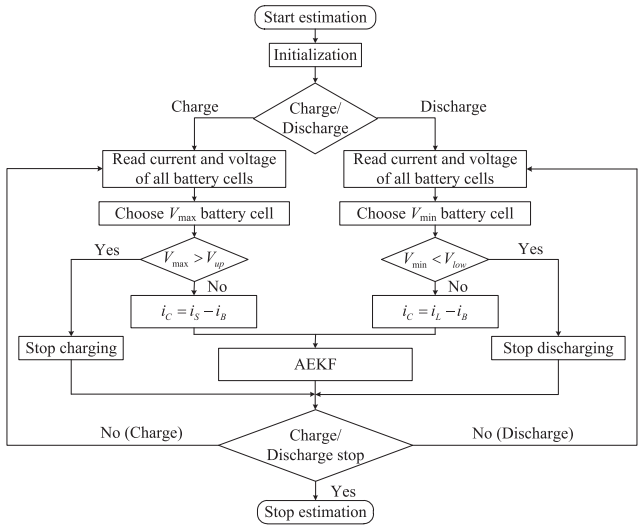

Fig. 8. Flowchart of the proposed approach.

During the correction step, AEKF gives the state and covariance correction as follows:

$$\hat{x}^+_k=\hat{x}^-_k+L_k[y'_k-h(\hat{x}^-_k,u_k)] \tag{33}$$

$$\Sigma^+_{x_k}=(I-L_kC_k)\Sigma^-_{x_k} \tag{34}$$

where y'_k is the measured terminal voltage of Cell #*n* at time *k*.

AEKF adjusts the covariance matrix Q_k and R_k at every time *k*. It is based on the innovation vector d_k, which is given by

$$d_k=y'_k-h(\hat{x}^-_k,u_k). \tag{35}$$

The estimation variance C_d of the innovation vector can be calculated as

$$C_{d_k}=\frac{k-1}{k}C_{d_{k-1}}+\frac{1}{k}d_kd^T_k,\qquad k\le W \tag{36}$$

$$C_{d_k}=\frac{1}{W}\sum_{i=k-W+1}^{k}d_id^T_i,\qquad k>W \tag{37}$$

where *W* is the length of moving window.

Then Q_k and R_k are updated as

$$Q_k=L_kC_{d_k}L^T_k \tag{38}$$

$$R_k=C_{d_k}-C_k\Sigma^-_{x_k}C^T_k+R_{k-1},\ R_{k,\min}\le R_k\le R_{k,\max} \tag{39}$$

where $R_{k,\min}$ and $R_{k,\max}$ are, respectively, the lower and upper limits of R_k.

B. Flowchart of the Proposed Approach

To summarize the procedure of the proposed approach, a detailed flowchart is shown in Fig. 8. $V_{\rm up}$ and $V_{\rm low}$ is the maximum and minimum limit voltage.

Although the battery is charged and discharged alternately in actual driving cycles, the SOC estimation is always based on the $V_{\min}$ cell. It is because that the pack is discharged most of the time. The duration of charging to recycle the braking energy is very limited, and the charging current is small compared to the

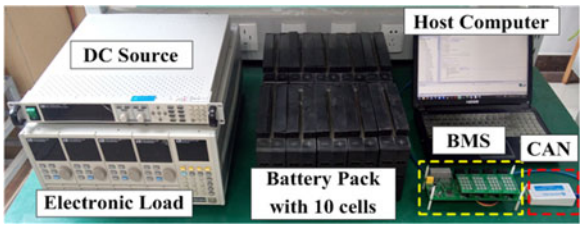

Fig. 9. Battery test bench.

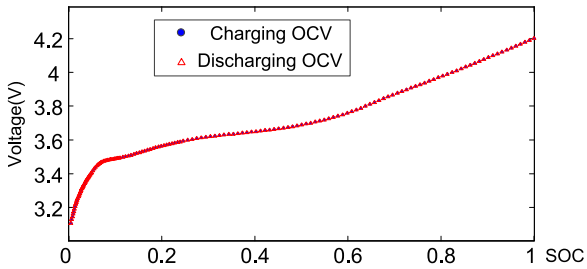

Fig. 10. OCV of the charging process and the discharging process.

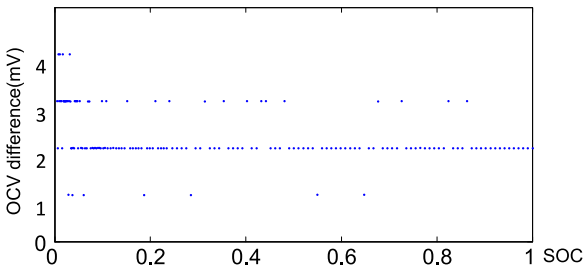

Fig. 11. OCV difference between the charging process and the discharging process.

discharging current. On the other hand, the capacity of battery in electric vehicles is normally very large. Therefore, the effect of the charging pulse is very limited, and it will not change the selection of $V_{\min}$ cell.

VI. Experimental Results and Discussion

The battery test bench was built as shown in Fig. 9. The battery pack contains ten series-connected Li(NiCoMn)O_2 batteries from Do-Fluoride New Energy Technology Co., Ltd. The nominal capacity and rated voltage of each cell are 200 Ah and 3.6 V, respectively. The imbalanced cells are balanced by the passive equalization circuits, and the balancing resistance is 13 Ω. The electronic load and the dc source are IT8732 and IT6512 from ITECH. They are programmed to discharge and charge the battery pack.

A. Battery Parameters Test

The OCV of each cell is measured after the pulse charging and discharging with 50 A and relaxation for 1 h. Take Cell #1 as example: the OCV for the charging and discharging process is shown in Fig. 10, and the number of data points is 152.

The OCV difference is presented in Fig. 11. It can be observed that the OCV difference is less than 3 mV except for several data points in low SOC status. The OCV difference of other

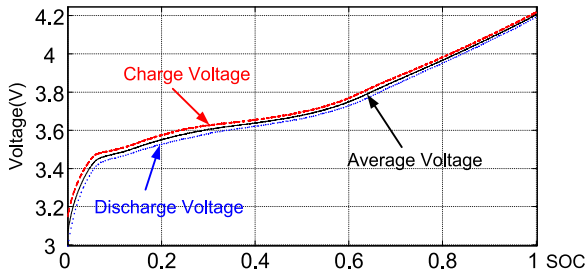

Fig. 12. Measured OCV–SOC curve.

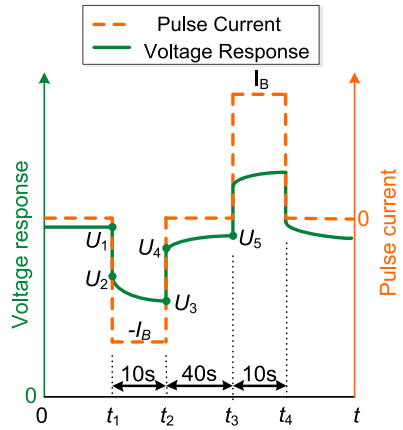

Fig. 13. Current and voltage profile of the HPPC test.

cells shows the similar results. Therefore, the hysteresis effect is ignored and the OCV is determined by interpolation here.

To simplify the model, the battery cell is charged and discharged with 8 A continuously. The duration is not long so that the self-discharge is ignored here. Take Cell #1 as example: the OCV can be obtained by calculating the average voltage of the charging and discharging voltage, as shown in Fig. 12.

Using MATLAB curve-fitting tool, it is found that the OCV function of Cell #1 can be approximated perfectly by the eighth-order polynomial, as given in (40). The root-mean-squared error can be limited to 0.0054

$$\begin{aligned} u_{\mathrm{OCV}} = &-465.5 \cdot \mathrm{SOC}^8 + 1998 \cdot \mathrm{SOC}^7 - 3538 \cdot \mathrm{SOC}^6 \\ &+ 3335 \cdot \mathrm{SOC}^5 - 1805 \cdot \mathrm{SOC}^4 + 567.4 \cdot \mathrm{SOC}^3 \\ &- 100.5 \cdot \mathrm{SOC}^2 + 9.7 \cdot \mathrm{SOC} + 3.106. \end{aligned} \tag{40}$$

Other battery parameters such as the internal resistance, polarization resistances, and polarization capacitances can be identified by the hybrid pulse power characteristic (HPPC) test. The pulse current profile of HPPC test and the voltage response of the battery cell are shown in Fig. 13.

The voltage response of the battery cell is sampled, and it is used to identify the cell parameters by MATLAB Curve Fitting Tool. The temperature has effect on battery parameters. In this experiment, the temperature is remained at room temperature. Therefore, the temperature has little effect on the battery parameters.

1) Measurement of R_O: In this experiment, the voltage sampling period is set to 50ms so that the sampling interval between

TABLE I
VARIATION OF PARAMETERS WITH SOC (CELL #1)

SOC (%)	R_O (mΩ)	R_D (mΩ)	C_D (mΩ)	R_T (mΩ)	C_T (F)
100	0.55	0.28	489 200	0.27	89 570
99	0.51	0.25	478 690	0.24	86 900
98	0.46	0.22	453 900	0.21	88 570
97	0.4	0.19	424 830	0.18	86 920
96	0.35	0.16	457 300	0.15	85 800
5–95	0.3	0.13	440 000	0.13	80 000
4	0.32	0.15	442 600	0.14	84 000
3	0.34	0.18	415 000	0.16	74 560
2	0.36	0.2	426 000	0.18	75 800
1	0.39	0.22	408 600	0.2	78 210
0	0.42	0.24	384 200	0.21	70 000

U_2 and U_1 is 50 ms. The voltage drop caused by the kinetic relaxation changes slowly, and it can be ignored. The internal resistance R_O can be measured by the voltage drop at t_1. It is described as

$$R_O = \frac{U_1 - U_2}{I_B} \tag{41}$$

where U_1 and U_2 are the measured voltage during HPPC test, as shown in Fig. 13, and I_B is the pulse current.

2) Measurement of R_D, R_T, C_D, and C_T:

In Fig. 13, there is a voltage rise from t_2 to t_3. It can be described as

$$u_B = U_5 - U_{O1} \cdot \exp(-t/\tau_D) - U_{O2} \cdot \exp(-t/\tau_T) \tag{42}$$

where U_{O1} and U_{O2} are the initial voltage of $R_D C_D$ and $R_T C_T$ circuits at t_2, and U_5 is the sampled voltage during HPPC test, as shown in Fig. 13. With the assistance of MATLAB Curve Fitting Tool, U_{O1}, U_{O2}, τ_D, and τ_T can be obtained.

From Fig. 13, it can be seen that there is a voltage drop from t_1 to t_2. It can be described as

$$\begin{aligned} u_B = U_2 &- \frac{\int I_B \cdot dt}{I_B \cdot T_{\text{interval}}/(U_1 - U_5)} \\ &- I_B \cdot R_D \cdot [1 - \exp(-t/\tau_D)] \\ &- I_B \cdot R_T \cdot [1 - \exp(-t/\tau_T)] \end{aligned} \tag{43}$$

where T_{interval} is the time interval between t_1 and t_2 and it is 10 s in this test. Based on τ_D and τ_T, R_D and R_T can be obtained with the assistance of MATLAB Curve Fitting Tool. Then C_D and C_T can be obtained according to τ_D, τ_T, R_D,and R_T.

Finally, the parameters of ten series-connected cells can be obtained. It should be noted that SOC affects the battery parameters. The parameters of the battery cells are measured at different SOC. It is found that the variation happens when the battery cell SOC is higher than 95% or lower than 5%. The parameters can be considered as constants when SOC is in range of 5%–95%. Take Cell #1 as example: the variation of parameters with SOC is listed in Table I.

When the cell SOC is in the extremes, the variation of parameters is simplified. The 1% SOC difference is divided into five equal pieces, and the parameters are set to five different values. Take Cell #1 as example: when SOC is in the range of 95%–96%, the variation of R_O is listed in Table II. The variation of other parameters is treated in the same manner.

TABLE II
VARIATION OF R_O IN THE SOC RANGE OF 95%–96% (CELL #1)

SOC (%)	95–95.2	95.2–95.4	95.4–95.6	95.6–95.8	95.8–96
R_O (mΩ)	0.31	0.32	0.33	0.34	0.35

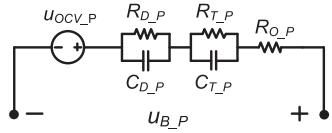

Fig. 14. Battery pack model.

TABLE III
BATTERY PACK PARAMETERS

OCV–SOC	$u_{\text{OCV\_P}} = -4646 \cdot \text{SOC}^8 + 19851 \cdot \text{SOC}^7 - 34977 \cdot \text{SOC}^6 + 32824 \cdot \text{SOC}^5 - 17713 \cdot \text{SOC}^4 + 5565 \cdot \text{SOC}^3 - 989 \cdot \text{SOC}^2 + 96 \cdot \text{SOC} + 31$				
Parameter	R_{O_P} (mΩ)	R_{D_P} (mΩ)	C_{D_P} (F)	R_{T_P} (mΩ)	C_{T_P} (F)
Value	3.2	1.5	48860	1.4	9240

B. Parameters of the Battery Pack Model

The battery pack model is shown in Fig. 14. $u_{\text{OCV\_P}}$ is OCV–SOC function. R_{O_P} is the internal resistance. R_{D_P}, R_{T_P}, C_{D_P}, and C_{T_P} are the polarization resistances and capacitances. u_{B_P} is the terminal voltage.

The parameters of the pack model can be identified by HPPC test. The OCV–SOC function and the pack parameters are given in Table III.

C. Experiment Testing

For the charging process, the threshold of voltage difference is set to 20 mV, and the charging current is set to 20 A. The terminal voltage of each cell is shown in Fig. 15. For a clear comparison, the zoomed figure is presented in Fig. 15(b). The maximum voltage difference is 218 mV, and the maximum SOC difference is 3.2% at the beginning of charging process. With the equalization, the voltage difference among cells is reduced.

Fig. 16(a) shows the dynamic selection of $V_{\max}$ cell during the charging process. The zoomed figure is presented in Fig. 16(b). It can be observed that the $V_{\max}$ battery cell swaps during the charging process.

The voltage difference between $V_{\max}$ and $V_{\min}$ is shown in Fig. 17. The passive equalization is completed at roughly 10 h. However, the equalization does not work from 10000 to 20000 s. Therefore, the equalization actually takes about 7 h. It is because that the threshold of voltage difference is set to 20 mV (2.2% SOC difference). The capacity difference that needs to be balanced is about 2 Ah, which is 3.2% − 2.2% = 1% SOC difference.

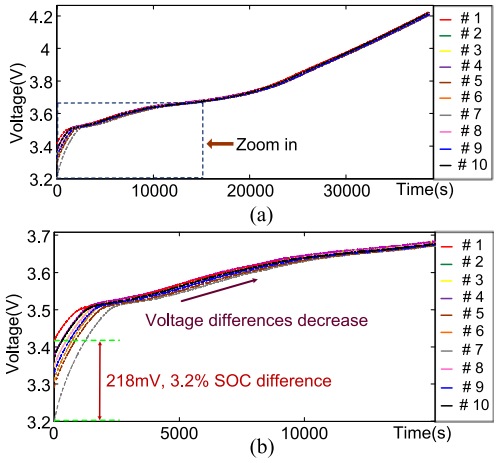

Fig. 15. (a) Terminal voltage of each cell in charging process. (b) Zoomed terminal voltage of each cell in charging process.

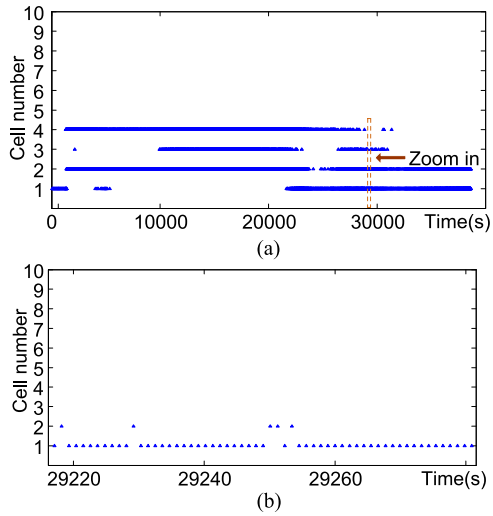

Fig. 16. (a) $V_{\max}$ cell number in charging process. (b) Zoomed $V_{\max}$ cell number in charging process.

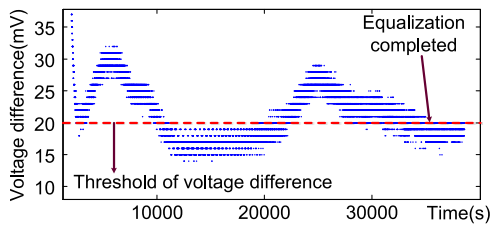

Fig. 17. Voltage difference between $V_{\max}$ and $V_{\min}$ during charging process.

For the discharging process, the battery pack is discharged under the Urban Dynamometer Driving Schedule (UDDS) driving cycle. Due to the limit of the electronic load, the charging pulse is not included and the driving cycle is simplified, as shown in Fig. 18.

The terminal voltage of each cell during the discharging process is shown in Fig. 19. For a clear comparison, the zoomed figure is presented in Fig. 19(b). The maximum voltage difference is 30 mV, and the maximum SOC difference is 3% at the beginning of the discharging process. The passive equalization

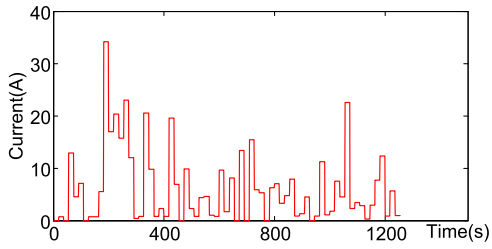

Fig. 18. Simplified UDDS driving cycle.

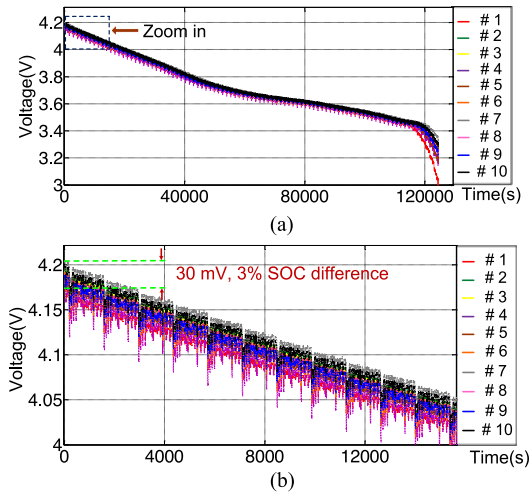

Fig. 19. (a) Terminal voltage of each cell in discharging process. (b) Zoomed terminal voltage of each cell in discharging process.

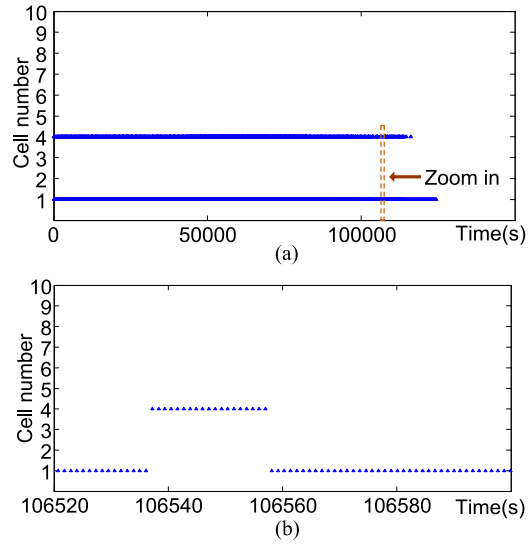

Fig. 20. (a) $V_{\min}$ cell number in discharging process. (b) Zoomed $V_{\min}$ cell number in discharging process.

is not applied in the discharging process so that the voltage difference among battery cells cannot be decreased.

Fig. 20(a) shows the dynamic selection of $V_{\min}$ cell during the discharging process. The zoomed figure is presented in Fig. 20(b). It can be observed that the $V_{\min}$ battery cell swaps during the discharging process.

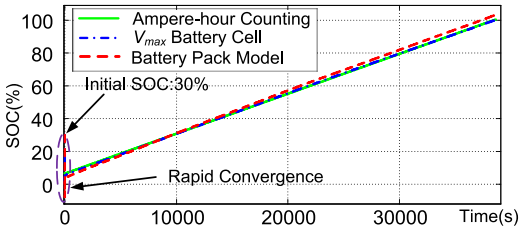

Fig. 21. SOC estimation based on battery pack model and $V_{\max}$ battery cell.

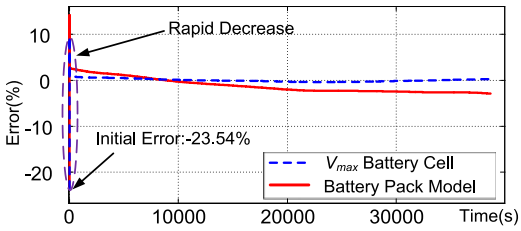

Fig. 22. SOC estimation error based on battery pack model and $V_{\max}$ battery cell.

D. Comparison Between Battery Pack Model and Proposed Method

1) Comparison Between Battery Pack Model and $V_{\max}$ Battery Cell During Charging Process: During the charging process, the pack SOC should be based on $V_{\max}$ cell. The INA226 current shunt monitor chip from Texas Instruments is used to measure the charging current. The balancing current is calculated with the cell voltage and the balancing resistance considering the voltage drop generated by other devices. The ampere–hour counting considering the balancing current can be used as the benchmark. The SOC estimation comparison between the pack model and $V_{\max}$ cell during the charging process is shown in Fig. 21. In order to validate the robustness of the proposed approach, the initial SOC is set to 30%, while true SOC is 6.46%. It is observed that the estimated SOC based on AEKF converges to true SOC quickly.

The comparison of SOC estimation error between pack model and $V_{\max}$ cell during the charging process is shown in Fig. 22. It can be observed that the initial error is 23.54% and the error decreases rapidly in the following several seconds. Meanwhile, it is noted that the SOC estimation based on $V_{\max}$ cell shows better performance than that based on pack model. This is due to the following two factors: 1) the pack model ignores the difference among cells; and 2) the balancing current is ignored in the pack model, while the voltage of the pack and string current are used to estimate the pack SOC.

For a convenient comparison, the zoomed figure of SOC estimation error is shown in Fig. 23. It can be observed that for AEKF based on $V_{\max}$ cell, the maximum estimation error is 0.3%. Compared to the maximum estimation error of 2.8% for AEKF based on the pack model, an estimation error reduction of 2.5% can be obtained.

2) Comparison Between the Battery Pack Model and $V_{\min}$ Battery Cell During the Discharging Process: During the discharging process, the SOC estimation of the battery pack should be based on $V_{\min}$ cell. The SOC estimation comparison between

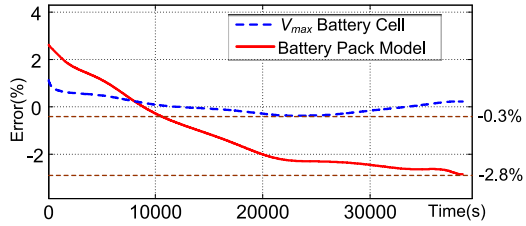

Fig. 23. Zoomed SOC estimation error based on battery pack model and $V_{\max}$ battery cell.

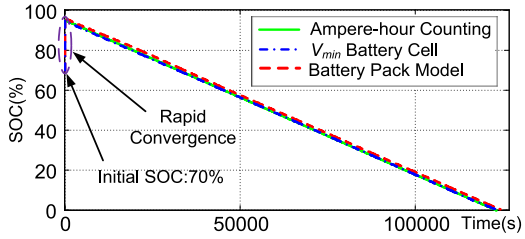

Fig. 24. SOC estimation based on battery pack model and $V_{\min}$ battery cell.

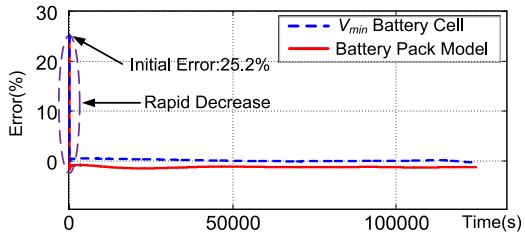

Fig. 25. SOC estimation error based on battery pack model and $V_{\min}$ battery cell.

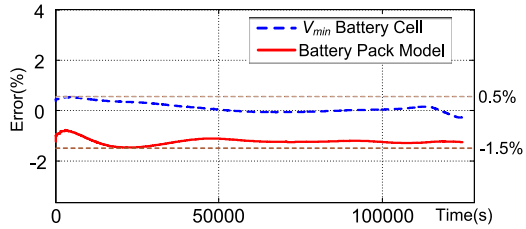

Fig. 26. Zoomed SOC estimation error based on battery pack model and $V_{\min}$ battery cell.

pack model and $V_{\min}$ cell during the discharging process is shown in Fig. 24. In order to validate the robustness, the initial SOC is set to 70%, while the true SOC is 95.2%.

The comparison of SOC estimation error between the pack model and $V_{\min}$ cell during the discharging process is shown in Fig. 25. It can be observed that the initial error is 25.2% and the error decreases rapidly in the following several seconds. The SOC estimation error of AEKF based on $V_{\min}$ cell is smaller than AEKF based on the pack model.

The zoomed figure of SOC estimation error is shown in Fig. 26. It can be seen that AEKF based on $V_{\min}$ cell achieves better performance over the AEKF based on the pack model. For AEKF based on $V_{\min}$ cell, the maximum estimation error is 0.5%. Compared to the error of 1.5% for AEKF based on the pack model, an estimation error reduction of 1% is achieved. The passive equalization is not applied during the discharging

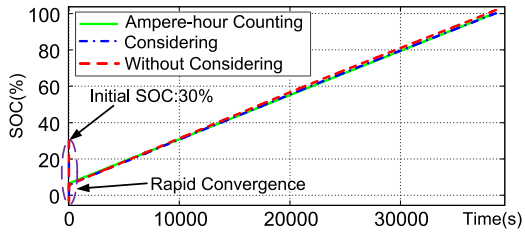

Fig. 27. SOC estimation of $V_{\max}$ cell with and without considering the balancing current.

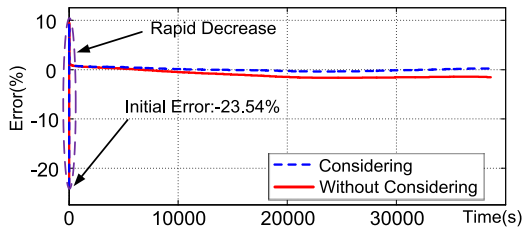

Fig. 28. SOC estimation error of $V_{\max}$ cell with and without considering the balancing current.

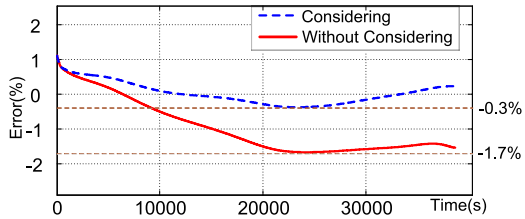

Fig. 29. Zoomed SOC estimation error of $V_{\max}$ cell with and without considering the balancing current.

process so that the current of $V_{\min}$ cell is equal to the string current. In this case, the SOC estimation error is caused by small difference of *RC* parameters and OCV–SOC functions among cells. The pack model ignores such differences so that the approach based on the pack model has lower accuracy on SOC estimation.

E. Comparison Between $V_{\max}$ Cell With and Without Considering the Balancing Current

To verify the proposed approach, SOC estimation comparison between AEKF with and without considering balancing current is carried out during the charging process. The SOC estimation comparison of $V_{\max}$ cell with and without considering balancing current is shown in Fig. 27. In order to validate the robustness, the initial SOC is set to 30%, while true SOC is 6.46%.

The SOC estimation error comparison of $V_{\max}$ cell with and without considering balancing current is shown in Fig. 28. It can be observed that the initial error is 23.5% and the error decreases rapidly in the following several seconds. Meanwhile, it is noted that SOC estimation error of $V_{\max}$ cell considering balancing current is smaller than that without considering balancing current.

The zoomed figure of SOC estimation error is shown in Fig. 29. It can be seen that AEKF considering balancing current achieves better performance than AEKF without considering balancing current. For AEKF considering balancing current, the maximum estimation error is 0.3%. Compared to an error of 1.7% for AEKF without considering balancing current, an error reduction of 1.4% can be obtained.

VII. Conculsion

The SOC estimation approaches based on pack model ignore the difference among cells. On the other hand, the approaches based on each cell increase the computing resource cost and calculation time, which is not suitable for real-time application. Meanwhile, the balancing current in the equalization circuit has effects on cell SOC estimation. In this paper, the SOC estimation approach of battery pack considering balancing current is proposed. This approach dynamically searches for $V_{\max}$ or $V_{\min}$ cell. The pack SOC estimation is based on $V_{\max}$ cell in charging process and $V_{\min}$ cell in discharging process. The balancing current has also been taken into consideration in AEKF, which increases accuracy of SOC estimation. Compared to SOC estimation approaches based on the pack model or each cell, this approach can achieve precise pack SOC and reduce calculation time. It has been validated by experimental results on 10 series-connected Li(NiCoMn)O_2 batteries. Each battery cell has the rated capacity of 200 Ah and rated voltage of 3.6 V. With the proposed approach, SOC estimation error is limited within 0.3% during the charging process. Compared to an error of 2.8% based on the pack model, an error reduction of 2.5% is achieved. An error reduction of 1% is achieved compared to an error of 1.5% based on the pack model during the discharging process. Compared to an error of 1.7% without considering balancing current, an error reduction of 1.4% is achieved during the charging process.

Reference

[1] H. R. Eichi, F. Baronti, and M. Y. Chow, "Online adaptive parameter identification and state-of-charge coestimation for Lithium-polymer battery cells," *IEEE Trans. Ind. Electron.*, vol. 61, no. 4, pp. 2053–2061, Apr. 2014.

[2] J. Kim, J. Shin, C. Chun, and B. H. Cho, "Stable configuration of a Li-ion series battery pack based on a screening process for improved voltage SOC balancing," *IEEE Trans. Power Electron.*, vol. 27, no. 1, pp. 411–424, Jan. 2012.

[3] J. Kim, "Discrete wavelet transform-based feature extraction of experimental voltage signal for Li-ion cell consistency," *IEEE Trans. Veh. Technol.*, vol. 65, no. 3, pp. 1150–1161, Mar. 2016.

[4] L. Y. Wang, M. P. Polis, G. G. Yin, W. Chen, Y. H. Fu, and C. C. Mi, "Battery cell identification and SOC estimation using string terminal voltage measurements," *IEEE Trans. Veh. Technol.*, vol. 61, no. 7, pp. 2925–2935, Sep. 2012.

[5] X. F. Lin, A. G. Stefanopoulou, Y. H. Li, and R. D. Anderson, "State of charge imbalance estimation for battery strings under reduced voltage sensing," *IEEE Trans. Control Syst. Technol.*, vol. 23, no. 3, pp. 1052–1062, May 2015.

[6] M. A. Roscher, O. S. Bohlen, and D. U. Sauer, "Reliable state estimation of multicell Lithium-ion battery systems," *IEEE Trans. Energy Convers.*, vol. 26, no. 3, pp. 737–743, Sep. 2011.

[7] A. M. Imtiaz and F. H. Khan, "Time shared flyback converter based regenerative cell balancing technique for series connected Li-ion battery strings," *IEEE Trans. Power Electron.*, vol. 28, no. 12, pp. 5960–5975, Dec. 2013.

[8] C. H. Kim, M. Y. Kim, H. S. Park, and G. W. Moo, "A modularized two-stage charge equalizer with cell selection switches for series-connected Lithium-ion battery string in an HEV," *IEEE Trans. Power Electron.*, vol. 27, no. 8, pp. 3764–3774, Aug. 2012.

[9] M. Y. Kim, J. H. Kim, and G. W. Moon, "Center-cell concentration structure of a cell-to-cell balancing circuit with a reduced number of switches," *IEEE Trans. Power Electron.*, vol. 29, no. 10, pp. 5285–5297, Oct. 2014.
[10] S. H. Park, K. B. Park, H. S. Kim, G. W. Moon, and M. J. Youn, "Single-magnetic cell-to-cell charge equalization converter with reduced number of transformer windings," *IEEE Trans. Power Electron.*, vol. 27, no. 6, pp. 2900–2911, Jun. 2012.
[11] Z. Zhang, H. D. Gui, D. J. Gu, Y. Yang, and X. Ren, "A hierarchical active balancing architecture for lithium-ion batteries," *IEEE Trans. Power Electron.*, vol. 32, no. 4, pp. 2757–2768, Apr. 2017.
[12] Y. L. Shang, C. H. Zhang, N. X. Cui, and J. M. Guerrero, "A cell-to-cell battery equalizer with zero-current switching and zero-voltage gap based on quasi-resonant LC converter and boost converter," *IEEE Trans. Power Electron.*, vol. 30, no. 7, pp. 3731–3747, Jul. 2015.
[13] W. X. Huang and J. A. A. Qahouq, "Energy sharing control scheme for state-of-charge balancing of distributed battery energy storage system," *IEEE Trans. Ind. Electron.*, vol. 62, no. 5, pp. 2764–2776, May 2015.

Zhiliang Zhang (S'03–M'09–SM'14) received the B.Sc. and M.Sc. degrees in electrical engineering from Nanjing University of Aeronautics and Astronautics (NUAA), Nanjing, China, in 2002 and 2005, respectively, and the Ph.D. degree from the Department of Electrical and Computer Engineering, Queen's University, Kingston, ON, Canada, in 2009.

In June, 2009, he joined NUAA, where he is currently a Professor at the Aero-Power Sci-Tech Center. His current research interests include high-frequency power converters and renewable energy power conversion system.

Dr. Zhang was the Winner of the "United Technologies Corporation Rong Hong Endowment" in 1999. He was the Secretary of the PELS Technical Committee on Power and Control Core Technologies since 2013.

Xiang Cheng received the B.S. degree in electrical engineering in 2015 from Nanjing University of Aeronautics and Astronautics, Nanjing, China, where he is currently working toward the M.S. degree at the Aero-Power Sci-Tech Center.

His current research interests include renewable energy power converters.

Zhou-Yu Lu is currently working toward the B.S. degree in electrical engineering from Nanjing University of Aeronautics and Astronautics, Nanjing, China.

His current research interests include renewable energy power converters.

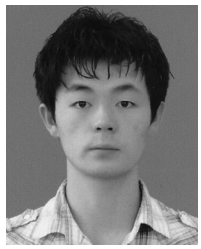

Dong-Jie Gu received the B.S. and M.Sc. degrees in electrical engineering from Nanjing University of Aeronautics and Astronautics, Nanjing, China, in 2014 and 2017, respectively.

He is currently with the Department of Power Electronics Center, Delta Electronics, Shanghai, China. His current research interests include renewable energy power converters.